catalysts

MDPI

Article

Studies on the Binary MgO/SiO_2 Mixed Oxide Catalysts for the Conversion of Ethanol to 1,3-Butadiene

Wladimir Reschetilowski [1,*], Matthias Hauser [2,*], Felix Alscher [1], Mandy Klauck [2] and Grit Kalies [2]

[1] Faculty of Chemistry and Food Chemistry, Dresden University of Technology, Mommsenstrasse 4, D-01062 Dresden, Germany; felix.alscher@tu-dresden.de

[2] Department Chemical Engineering, HTW University of Applied Sciences Dresden, Friedrich-List-Platz 1, D-01069 Dresden, Germany; mandy.klauck@htw-dresden.de (M.K.); grit.kalies@htw-dresden.de (G.K.)

* Correspondence: Wladimir.Reschetilowski@tu-dresden.de (W.R.); matthias.hauser@htw-dresden.de (M.H.)

Received: 1 July 2020; Accepted: 25 July 2020; Published: 1 August 2020

Abstract: The demand for 1,3-butadiene, one of the most important raw materials in the rubber industry, is constantly increasing. The Lebedev process is a classical method of producing 1,3-butadiene from ethanol, which is to be optimized with regard to the mixed oxide catalysts used. In this work, the binary MgO/SiO_2 solid system was tested with regard to its optimum chemical composition for the catalytic conversion of ethanol to 1,3-butadiene. Furthermore, novel mesoporous mixed oxides were prepared to investigate their textural, structural, and surface chemical properties as well as the catalytic activity. Nitrogen physisorption, scanning electron microscopy (SEM), and temperature-programmed ammonia desorption (NH_3-TPD) measurements were carried out and evaluated. It was shown that the optimum yield of 1,3-butadiene is achieved by using MgO/SiO_2 mixed oxide catalysts with 85–95 mol% MgO and not, as suggested by Lebedev, with 75 mol% MgO. The NH_3-TPD measurements revealed that the maximum acid-site density is achieved with an equimolar up to magnesium-rich composition. During the synthesis of binary MgO/SiO_2 solid systems based on mesoporous MgO, a thermally stable and ordered structure was formed in the autoclave, depending on the carbonate used and on the duration of the treatment.

Keywords: butadiene; characterization; heterogeneous catalysis; mesoporous materials; mixed oxide catalyst

1. Introduction

Fossil raw materials such as petrol, natural gas, and coal are important sources for fuel production and the chemical industry [1,2]. In recent years, complex mining methods such as the MultiFrac method (fracking) have been increasingly used [3]. This has an impact on the availability and price of one of the most important raw materials in the rubber industry, namely 1,3-butadiene [4].

The large number of polymers synthesized from 1,3-butadiene provides a diverse range of products, with more than half of the end products found in the tire and seal industries [4]. The consumption of synthetically produced rubber in 2018 was about 15.4 million tons [5]. An overview of the processing of 1,3-butadiene and the application of the end products is given in the Appendix A (see Table A1).

Around 95% of the 1,3-butadiene demand is currently covered by steam cracking for the production of short-chain olefins [4]. However, the amount of 1,3-butadiene recovered depends strongly on the petrochemical raw material used. Utilizing the petroleum fractions naphtha or gas oil, the product stream contains about 9 vol% C_4 hydrocarbons with a 1,3-butadiene content of 30–60% [6,7]. However, the use of shale gas with a high ethane content as a feedstock for steam cracking results in a lower

1,3-butadiene content in the product stream [8]. A production based on renewable raw materials and independent of fossil raw materials is therefore desirable [9].

An interesting alternative to the petrochemical production of 1,3-butadiene is the Lebedev process, as it is based on the use of ethanol obtained from fermentation as a biobased raw material [10]. This process has been known since the 1930s [11], but lost importance due to the development of petrochemistry and the relatively inexpensive production by steam cracking.

The total reaction equation of the conversion of ethanol to 1,3-butadiene is shown in Scheme 1. The generally accepted scheme of the reaction process is shown in Scheme 2 [12–16].

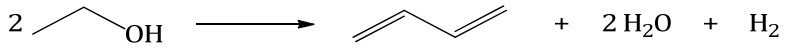

Scheme 1. Total reaction equation of the conversion of ethanol to 1,3-butadiene.

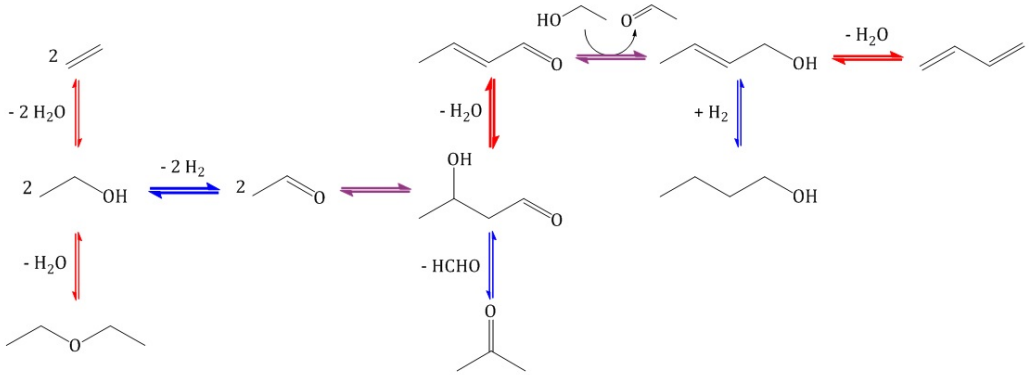

Scheme 2. Reaction scheme of the conversion of ethanol to 1,3-butadiene. Blue arrows: basic catalyzed reaction. Red arrows: acidic catalyzed reaction. Violet arrows: acidic and/or basic catalyzed reaction.

In the first step, ethanol is dehydrated to acetaldehyde. This requires a catalyst with active basic sites. The intermediate product acetaldol is then formed by the aldol addition of two acetaldehyde molecules. It is known from homogeneously catalyzed liquid-phase reactions that this reaction can take place with both basic and acidic catalysts [17]. Therefore, the same is assumed for the heterogeneous catalyzed gas-phase reaction [18] presented in this paper. The subsequent dehydration to crotonaldehyde takes place at acid sites. The mono-unsaturated crotonaldehyde is reduced to alcohol in the next step. In this case, however, hydrogenation is not carried out directly with hydrogen, but via a Meerwein-Ponndorf-Verley reduction with simultaneous dehydrogenation of ethanol to acetaldehyde at the adjacent strongly basic and weakly acid surface sites [19,20]. In the last step, the desired product 1,3-butadiene is formed from crotyl alcohol by further dehydration at acid sites of the catalyst.

In the literature, different statements can be found regarding the rate-determining step in this multi-step reaction scheme to the formation of 1,3-butadiene. On the one hand, the dehydrogenation of ethanol to acetaldehyde is mentioned as the limiting reaction step [21] and, on the other hand, the aldol reaction to build up the C_4 chain [19].

In view of the large number of basic and acidic catalyzed reactions during the conversion of ethanol to 1,3-butadiene, the necessity of using a multifunctional catalyst with very defined properties in this case becomes clear. The Lebedev process uses heterogeneous mixed oxide catalysts with the basic and acidic surface properties required for the conversion of ethanol [14]. The quantity and strength of the basic and acid sites can be controlled by selecting the oxidic compounds. The ratio of these active sites can be adjusted by the proportions of the respective components in the mixed oxide [16].

According to Lebedev, a mixed oxide catalyst consisting of 75 mol% dehydrogenation (basic) and 25 mol% dehydration (acidic) components should be used for the selective formation of

1,3-butadiene [11]. In the early 1930s, Lebedev patented the combination of magnesium oxide and silicon dioxide as a catalyst system for the production of 1,3-butadiene in a single-step process [22]. To date, MgO/SiO_2 is the most promising binary mixed oxide for 1,3-butadiene synthesis from ethanol [12,15,16,23–28]. The yield of 1,3-butadiene depends strongly on the chosen reaction conditions. The most frequent by-product is ethene formed at the acid sites. With regard to the yield of 1,3-butadiene, different data can be found on the optimum Mg/Si ratio of the binary catalyst. However, a high MgO content of 75 to 85 mol% is often recommended [21,27,29], even though lower MgO contents of 65 mol% have also been reported [30]. In recent times, the role of the multifunctionality of the catalyst systems used separately has also been studied more closely [31–33].

In the present study, the molar composition of the binary MgO/SiO_2 mixed oxides was investigated and confirmed or optimized to achieve high 1,3-butadiene yields. New mixed oxide systems with an optimal MgO/SiO_2 ratio were produced with mesoporous MgO. Special emphasis was placed on an extensive variation of the precipitation reagents and the duration of hydrothermal treatment during the production of mesoporous magnesium oxides. The obtained systems were subjected to systematic textural, structural, and surface chemical characterization. Their suitability as effective catalysts for the heterogeneous catalyzed conversion of ethanol to 1,3-butadiene was demonstrated.

2. Results and Discussion

2.1. Binary MgO/SiO_2 Mixed Oxides from Commercially Available Precursors

2.1.1. Characterization

The adsorption isotherms for the precursors M1 and SiO_2 treated according to Section 3.2. and for the correspondingly prepared binary mixed oxides are shown in Figures 1 and 2.

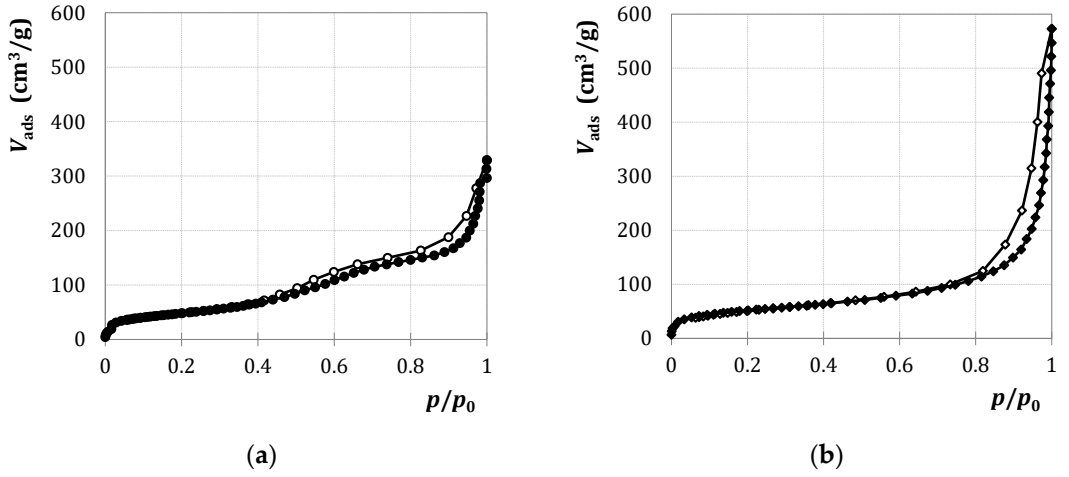

Figure 1. Nitrogen adsorption and desorption at 77 K on (**a**) M1 and (**b**) SiO_2.

Both adsorption isotherms in Figure 1, i.e., the type IV(a) isotherm of M1 and the type II isotherm of SiO_2 according to IUPAC [34], exhibit a small hysteresis in the relative pressure range from 0.8 to 1.0, which is probably more a result of the intermediate particle volume than of the presence of a mesopore system. M1 can therefore be regarded as slightly mesoporous and SiO_2 as macroporous as well as nonporous.

The isotherms of the mixed oxides in Figure 2 are of type IV(a) with an adsorption hysteresis, whereby the adsorption capacity decreases with increasing MgO content. The hysteresis of type H2(b) [34] indicates a broad, heterogeneous pore-size distribution. For the mixed oxides $M1/SiO_2$ 25:75 and $M1/SiO_2$ 50:50, the adsorbed volume increases strongly at low relative pressures. This points to a certain content of micropores in addition to mesopores.

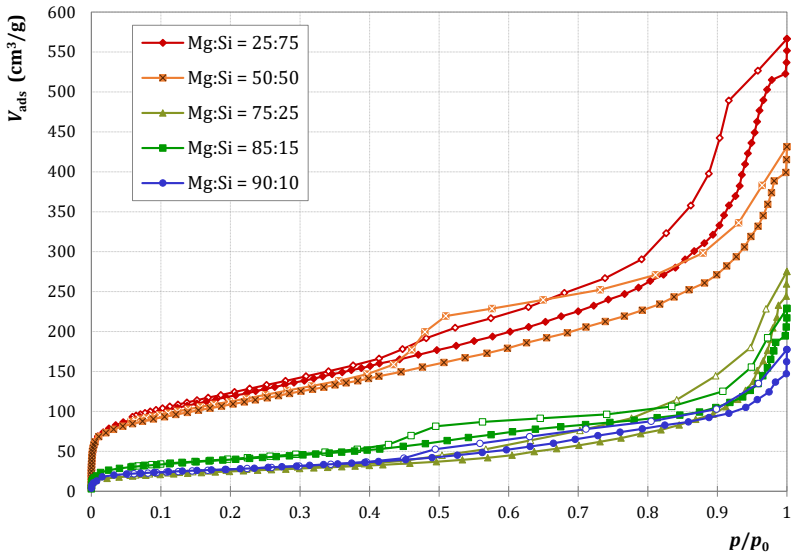

Figure 2. Nitrogen adsorption and desorption at 77 K on M1/SiO_2 mixed oxide samples with various compositions.

The textural parameters determined from the adsorption isotherms are listed in Table 1. In order to calculate the specific surface area S_{BET}, the Brunauer-Emmett-Teller (BET) equation was linearized in the relative pressure range from 0.05 to 0.25. The specific pore volume V_p was calculated from the adsorbed amount of nitrogen at a relative pressure of 0.95, using the molar volume of gaseous and liquid nitrogen [34].

Table 1. Textural properties of binary M1/SiO_2 mixed oxides and of the precursors M1 and SiO_2.

MgO Content (mol%)	0	25	50	75	85	90	100
S_{BET} (m^2/g)	185	432	391	90	143	98	174
V_p (cm^3/g)	0.31	0.67	0.49	0.20	0.20	0.16	0.29

While the precursors M1 and SiO_2 exhibit comparable textural parameters, S_{BET} and V_p of the mixed oxides sensitively depend on the MgO content. By far, the highest values are found for M1/SiO_2 25:75 and M1/SiO_2 50:50. Surprisingly, mixed oxides with high MgO contents show significantly smaller BET surface areas than the pure oxides.

The scanning electron microscopy (SEM) images of the precursors M1 and SiO_2 as well as the mixed oxide M1/SiO_2 90:10 are presented in Figures 3 and 4. M1 is characterized by platelet-shaped structures aligned with each other. A pore system forms between the platelets. SiO_2, however, consists of many small spherical particles with a diameter of about 20 to 30 nm, which agglomerates together.

In contrast to the pure oxide M1, the mixed oxide M1/SiO_2 90:10 (see Figure 4) is composed of rounded platelets. The significantly lower pore volume of M1/SiO_2 90:10 compared to M1 (see Table 1) may be caused by its changed morphology. In contrast to Figure 3b, no small spherical SiO_2 particles can be identified in Figure 4. The SiO_2 particles are probably distributed homogeneously over the MgO surface.

In Figure 5, the BET surface areas S_{BET}, ammonia loadings N_{NH_3}, and acid-site densities ρ_{as} of the oxide samples are presented as a function of the molar MgO content. The exact values are given in the Appendix A (see Table A2). The temperature-programmed ammonia desorption (NH_3-TPD) profiles as basis for calculating the ammonia loading are shown in Figure A1 in the Appendix A. M1 and SiO_2 show a lower ammonia loading N_{NH_3} and acid-site density ρ_{as} compared to the binary mixed oxides. However, N_{NH_3} of M1 is not zero, which indicates that the dehydrogenation component of the mixed oxide already has a few acid sites. The greater number of acid sites on the surface of the mixed oxides

may be explained by (i) the higher specific surface area generated as a result of the interaction of the two compounds that facilitates accessibility of acid sites and (ii) additional acid sites that are formed at the contact points of the two oxides.

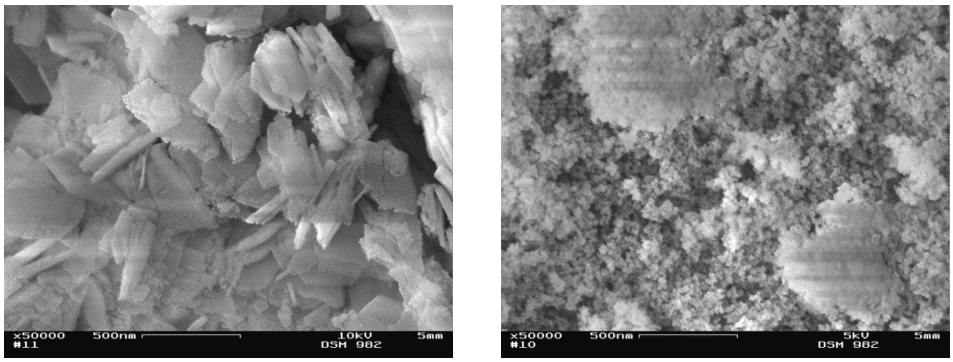

(**a**) (**b**)

Figure 3. Scanning electron microscopy (SEM) images of (**a**) M1 and (**b**) SiO_2 at 50,000× magnification.

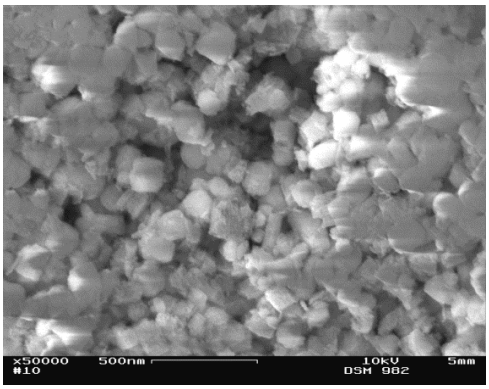

Figure 4. SEM image of M1/SiO_2 90:10 at 50,000× magnification.

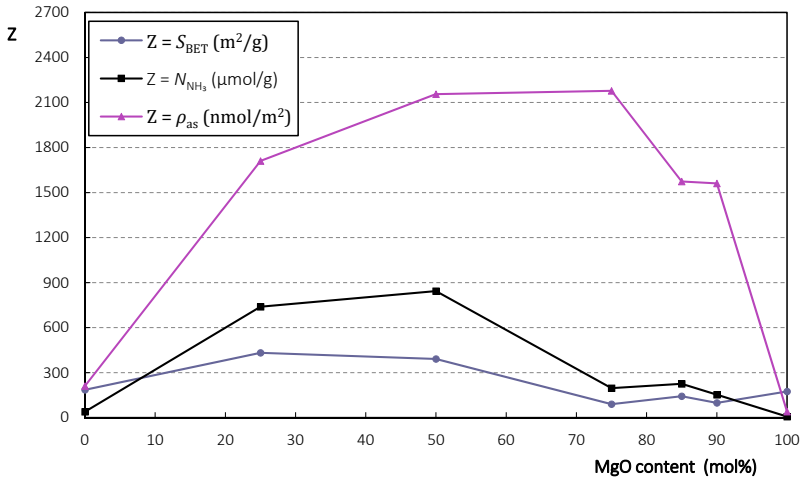

Figure 5. Characterization results of the textural and surface acid investigations on the binary M1/SiO_2 mixed oxides and the precursors M1 and SiO_2.

For the mixed oxides, N_{NH_3} and S_{BET} correlate, while the acid-site density ρ_{as} is slightly shifted in the direction of higher MgO contents.

2.1.2. Catalytic Testing

The results of the catalytic testing of the precursors M1 and SiO_2 as well as of the binary mixed oxides are illustrated in Figure 6. The conversion X of ethanol and the selectivities S_i to the respective product i (main product 1,3-butadiene, by-products, and intermediates) were calculated by the following:

$$X = \frac{n_{C,total} - n_{C,EtOH}}{n_{C,total}} \cdot 100\%, \quad (1)$$

$$S_i = \frac{n_{C,i}}{n_{C,total} - n_{C,EtOH}} \cdot 100\%. \quad (2)$$

Depending on the MgO content in the mixed oxide, the product distribution clearly shows two areas in the product spectrum, namely the formation of by-product ethene at low MgO contents and the formation of 1,3-butadiene at high MgO contents. The optimum yield of 1,3-butadiene was achieved with the mixed oxide M1/SiO_2 92.5:7.5, whereas Lebedev recommends a catalyst composition of 75 mol% dehydrogenation and 25 mol% dehydration components [11]. The recommended composition of M1/SiO_2 75:25 also produced 1,3-butadiene as main product, but the yield is significantly lower. At least Figure 6 confirms that the basic component in the mixed oxide must be present in excess.

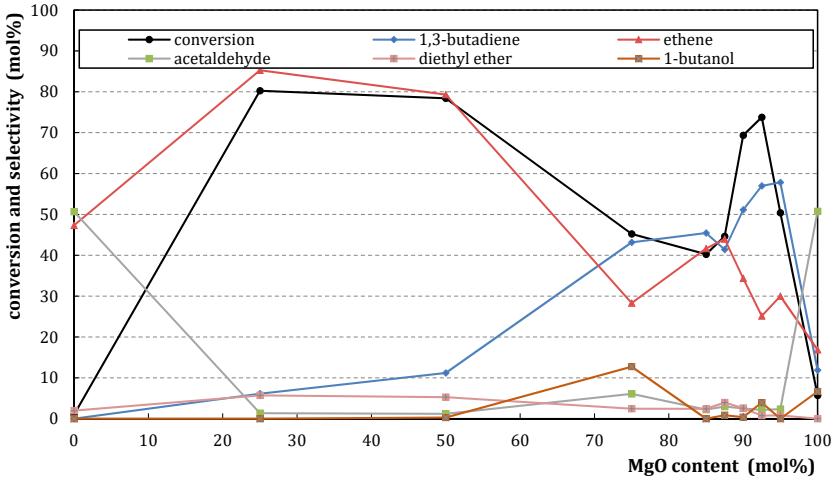

Figure 6. Results of catalytic testing of precursors M1 and SiO_2 and binary M1/SiO_2 mixed oxides with different molar composition; each produced according to Section 3.2. (m_{cat} = 500 mg; weight hourly space velocity (WHSV) = 1.2–1.8 h^{-1}; T = 450 °C; p = 5.5 bar(a); $\dot{V}_{N_2}$ = 5 L/h). Error bars have been omitted in favor of clarity.

The ratios of the selectivities S_{ethene}:$S_{acetaldehyde}$ and $S_{1,3\text{-butadiene}}$:$S_{1\text{-butanol}}$ are closely related to the ratio of acid to basic sites on the solid surface (see Scheme 2). Looking at the selectivities shown in Figure 6, the silicon-rich to equimolar mixed oxides show a ratio of acid to basic sites that is too high for an optimal 1,3-butadiene yield. However, the ratio for the samples with 75 mol% and 100 mol% MgO is too low. In the catalyst samples with 90 to 95 mol% MgO, the ratio of active sites seems to be very favorable for the 1,3-butadiene formation.

The presence of acid and basic sites on the catalyst surface is also necessary for the C_4 buildup by aldol condensation during the conversion of ethanol to 1,3-butadiene (see Scheme 2). Thus, both too low and too high ratios of acid to basic sites are disadvantageous for the C_4 buildup, as is the case with pure oxide M1 and binary mixed oxides with a high SiO_2 content.

A comparison of Figures 5 and 6 for the mixed oxides reveals a correlation between the BET surface area and the conversion. Only the sample M1/SiO_2 90:10 deviates from this trend with a high ethanol conversion, although it has a comparatively small BET surface area.

The low catalytic activity of pure SiO_2 with a conversion of ethanol of only 1 mol% is due to the comparatively small number of acid surface sites. Blank tests have shown that small amounts of

acetaldehyde are formed even without the presence of a catalyst (see Figure A2). Thus, the formation of ethene, but not the formation of acetaldehyde can be attributed to SiO_2. In contrast, pure M1 leads to the formation of acetaldehyde, ethene, and even C_4 products. This confirms the result of the temperature-programmed ammonia desorption (NH_3-TPD) measurements, according to which both basic and acid sites are present on the surface of M1.

2.2. Binary MgO/SiO_2 Mixed Oxides with Mesoporous MgO

2.2.1. Characterization

MgO precursors of the M2 series (synthesis according to Section 3.3, molar Mg/Si ratio of 90:10, precipitation with Na_2CO_3) were hydrothermally treated for either 0, 5, 12, or 24 h and then were used for the production of the mixed oxides. Figure 7a shows nitrogen adsorption at M2(0)/SiO_2 and Figure 7b shows it at M2(12)/SiO_2, which is similar to M2(5)/SiO_2 and M2(24)/SiO_2.

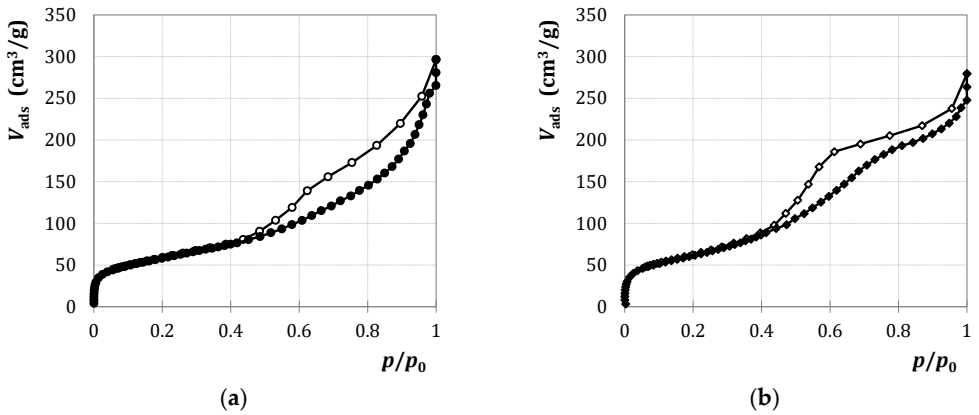

Figure 7. Nitrogen adsorption and desorption at 77 K on (**a**) M2(0)/SiO_2 90:10 and (**b**) M2(12)/SiO_2 90:10.

The adsorption isotherms of type IV(a) show a clear adsorption hysteresis, i.e., a mesoporous magnesium oxide is present in all samples as intended. For M2(0)/SiO_2, the hysteresis is almost a one-step, whereas for M2(5)/SiO_2, M2(12)/SiO_2, and M2(24)/SiO_2 it is rather two-step. The hysteresis curve indicates that M2(0)/SiO_2 has a larger amount of larger mesopores than the other samples.

In Table 2, the calculated specific BET surface areas and specific pore volumes are listed. The values are comparable, whereby S_{BET} increases slightly with the duration of the autoclave treatment.

Table 2. Textural properties of binary M2/SiO_2 90:10 mixed oxides.

Duration of Autoclave Treatment (h)	0	5	12	24
S_{BET} (m^2/g)	210	216	222	234
V_p (cm^3/g)	0.32	0.29	0.34	0.31

The SEM image of the M2(0)/SiO_2 sample is given in Figure 8. Disordered, platelet-shaped structures are visible. Accumulations of spherical SiO_2 particles are not visible. Again, it can be assumed that SiO_2 is distributed homogeneously in the mixed oxide.

The SEM images of the mixed oxides M2(5)/SiO_2 and M2(12)/SiO_2 are shown in Figure 9. A more ordered, platelet-shaped structure is formed, whereby the SiO_2 again appears to be distributed homogeneously over the structure. M2(12)/SiO_2 shows larger platelets than M2(5)/SiO_2, which indicates that the magnesium carbonate platelets continue growing during autoclave treatment at 180 °C. The treatment in the autoclave produces an increasingly ordered and stable structure, which is responsible for the mesoporous structure of the magnesium oxide M2 formed after calcination.

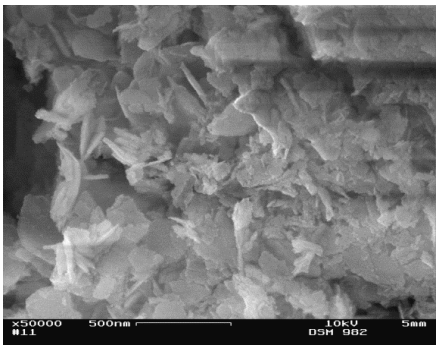

Figure 8. SEM image of M2(0)/SiO_2 90:10 at 50,000× magnification.

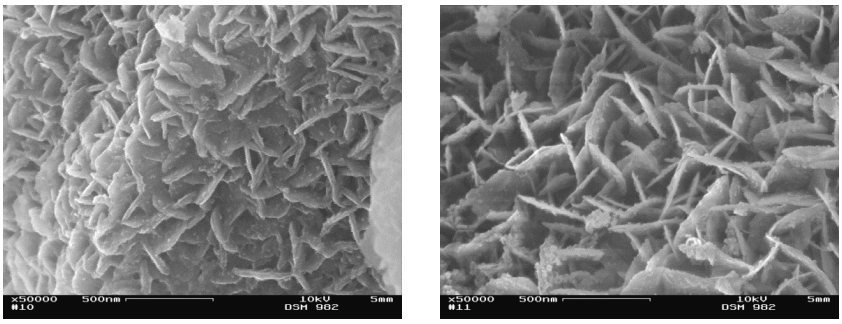

(**a**) (**b**)

Figure 9. SEM images of (**a**) M2(5)/SiO_2 90:10 and (**b**) M2(12)/SiO_2 90:10 at 50,000× magnification.

MgO precursors of the M3 series (synthesis according to Section 3.3., molar Mg/Si ratio of 90:10, precipitation with K_2CO_3) were hydrothermally treated for either 0, 5, 9, 12, 24, or 48 h before using them for the production of the mixed oxides. In Figure 10a, the nitrogen adsorption isotherm of M3(0)/SiO_2 is presented as being very similar to those of M3(5)/SiO_2 and M3(9)/SiO_2. Figure 10b shows nitrogen adsorption at M3(12)/SiO_2 similar to that at M3(24)/SiO_2 and M3(48)/SiO_2.

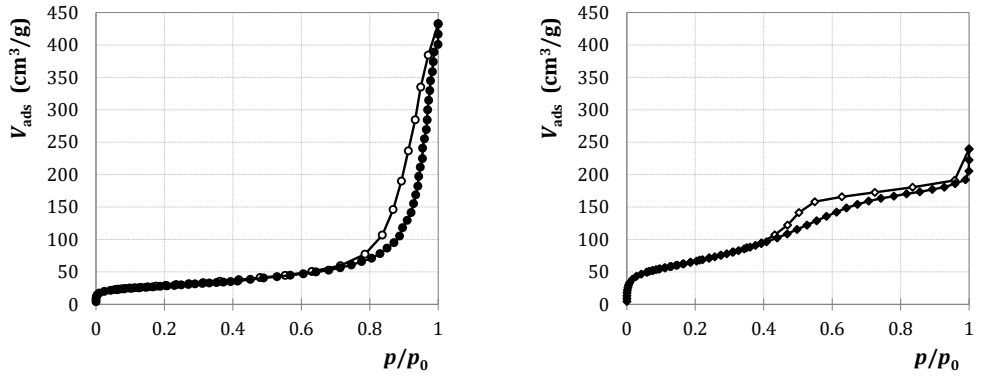

(**a**) (**b**)

Figure 10. Nitrogen adsorption and desorption at 77 K on (**a**) M3(0)/SiO_2 90:10 and (**b**) M3(12)/SiO_2 90:10.

The two isotherms in Figure 10 differ significantly. While the type II isotherm in Figure 10a indicates a rather macroporous to nonporous material with a certain intermediate particle volume, a type IV(a) isotherm characteristic for mesoporous materials can be found from a hydrothermal treatment of the MgO precursor of 12 h or longer. To illustrate the gain in mesopores, the calculated Barrett-Joyner-Halenda (BJH) pore radius distributions of the different M3/SiO_2 samples are shown in Figure A3.

Table 3 contains the calculated textural parameters of the M3/SiO_2 samples. In contrast to M2/SiO_2 (see Table 2), there is a significant increase in the BET surface areas of the mixed oxides with the duration of the autoclave treatment. A more ordered structure of $MgCO_3$ and thus of the resulting mixed oxide is presumably formed only after a treatment period of 12 h or longer.

Table 3. Textural properties of binary M3/SiO_2 90:10 mixed oxides.

Duration of Autoclave Treatment (h)	0	5	9	12	24	48
S_{BET} (m^2/g)	99	105	73	245	247	235
V_p (cm^3/g)	0.33	0.28	0.25	0.28	0.28	0.32

The SEM images in Figure 11 confirm this assumption. After autoclave treatment up to 9 h during the production of M3, a disordered platelet structure can be seen in the resulting mixed oxide. Treatment times of 12 h or longer lead to a defined order of the MgO platelets in the resulting mixed oxide, whereby in this case smaller SiO_2 accumulations are formed. With increasing duration of the autoclave treatment, the MgO platelets become larger and the order increases.

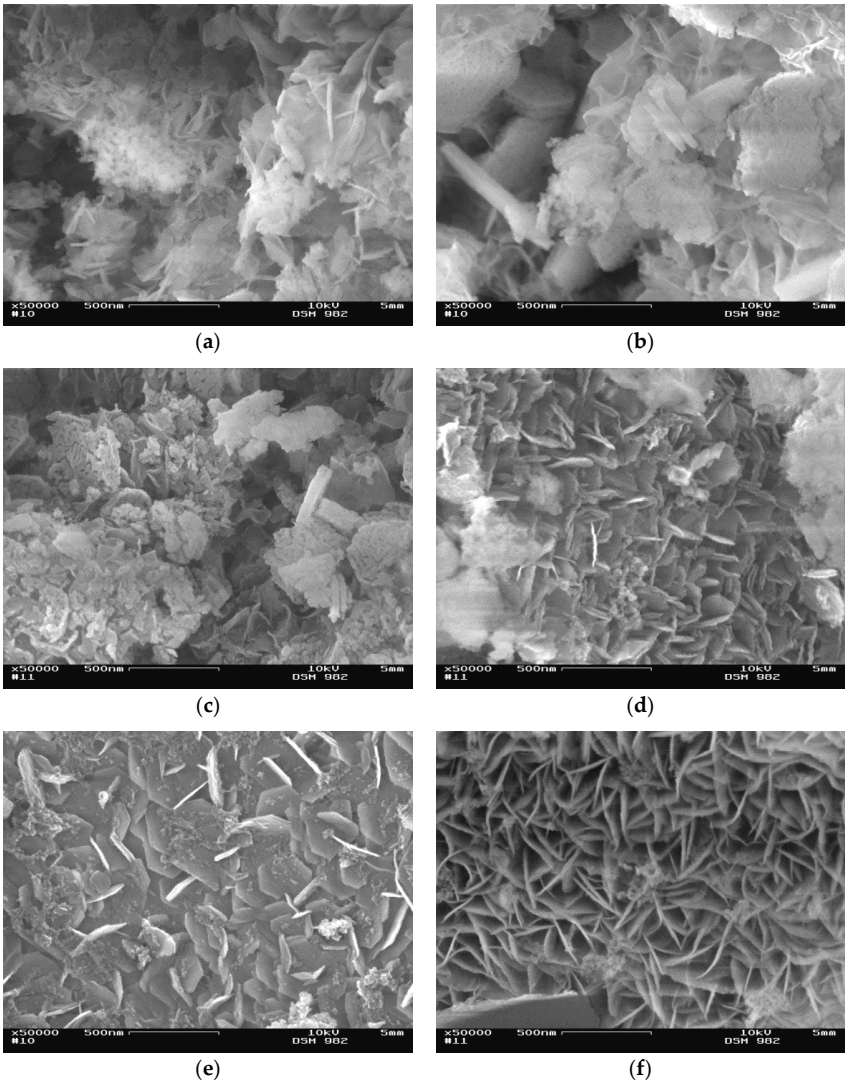

Figure 11. SEM images of M3/SiO_2 mixed oxides with (**a**) 0 h, (**b**) 5 h, (**c**) 9 h, (**d**) 12 h, (**e**) 24 h, (**f**) 48 h duration of autoclave treatment of the $MgCO_3$ precipitated suspension, at 50,000× magnification.

2.2.2. Catalytic Testing

The results of the catalytic testing of the M2/SiO_2 and M3/SiO_2 mixed oxides are presented in Figure 12. In both series, the conversion of ethanol and the selectivity to 1,3-butadiene are higher for samples whose MgO precursor was treated for at least 12 h in an autoclave.

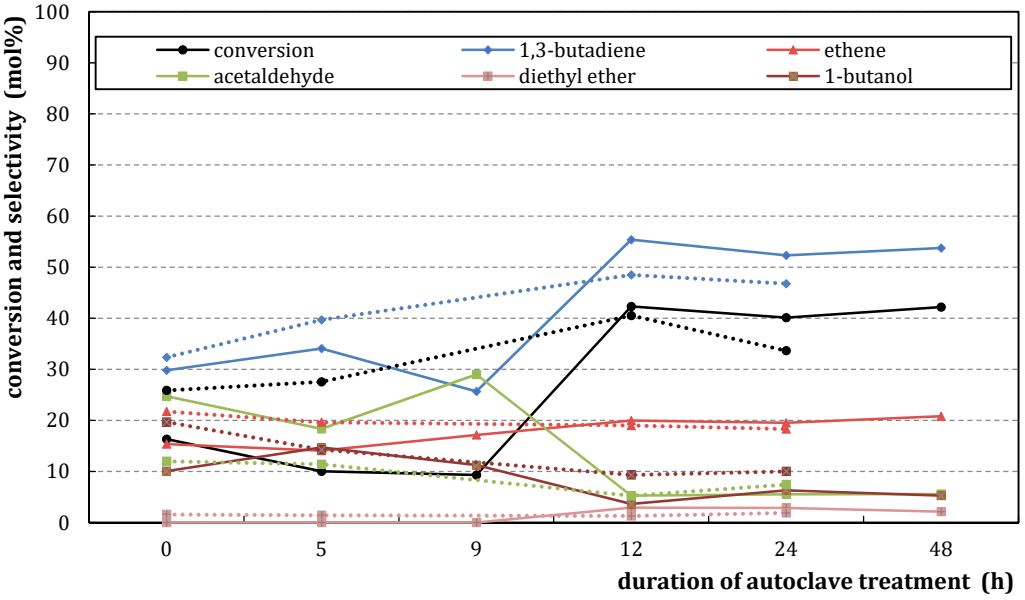

Figure 12. Results of catalytic testing of M2/SiO_2 90:10 (·····) and M3/SiO_2 90:10 (——); produced according to Section 3.3. with different autoclave treatment durations (m_{cat} = 500 mg; WHSV = 4.6–5.0 h^{-1}; T = 450 °C; p = 5.5 bar(a); $\dot{V}_{N_2}$ = 5 L/h). Error bars have been omitted in favor of clarity.

The samples of the M3/SiO_2 series, whose MgO precursor was treated up to 9 h in an autoclave, show conversions of ethanol of less than 20 mol% and selectivities to 1,3-butadiene between 25 and 35 mol%. Corresponding mixed oxides of the M2/SiO_2 series provide higher conversions of ethanol and slightly higher selectivities to 1,3-butadiene. Starting from an autoclave treatment time of $MgCO_3$ of 12 h, the corresponding mixed oxides of the M3/SiO_2 series cause significantly higher conversions of ethanol of about 40 mol% with simultaneously higher selectivities to 1,3-butadiene of more than 50 mol%. The mixed oxides of the M2/SiO_2 series show slightly less catalytic activity during the conversion of ethanol to 1,3-butadiene.

From the sum of the selectivities to 1,3-butadiene and 1-butanol in the M2/SiO_2 and M3/SiO_2 series, it becomes clear that the C_4 buildup on the mixed oxides is intensified if their MgO precursor has been treated for at least 12 h in the autoclave.

Figures 11 and 12 underline the conclusion that the mixed oxides with a more ordered structure and larger BET surface area cause a significantly greater conversion of ethanol and a higher selectivity to 1,3-butadiene. This is probably the result of a higher number of active sites on the larger MgO surface.

Tables 2 and 3 and Figure 12 illustrate that, in addition to the autoclave treatment time, the counter ion of the carbonate source in the precipitation suspension also influences the texture of the resulting MgO precursor and the formation of the catalytically active sites. In the presence of potassium ions, the formation of the stable $MgCO_3$ structure takes significantly longer than in the presence of sodium ions.

Differences in catalytic activity may also be caused by contamination of the mixed oxide with Na_2O or K_2O if the corresponding nitrate solution could not be completely removed in the preparation process by washing the $MgCO_3$ precipitate.

3. Materials and Methods

3.1. Chemicals Used

Table 4 lists the chemicals used to produce the mixed oxides. The MgO precursors synthesized in different ways are named M1, M2, and M3.

Table 4. Chemicals for the synthesis of mixed oxides.

Substance	Producer/Supplier (Product Number)	Application
$Mg(OH)_2$	Sigma-Aldrich, Taufkirchen, Germany (310093)	Synthesis of M1
$Mg(NO_3)_2{\cdot}6H_2O$	Grüssing, Filsum, Germany (12091250)	Synthesis of M2 and M3
Na_2CO_3	Grüssing, Filsum, Germany (12117)	Synthesis of M2
K_2CO_3	Grüssing, Filsum, Germany (12005)	Synthesis of M3
SiO_2	Wacker Silicones, Burghausen, Germany (HDK N20)	SiO_2 precursor

The deionized water, which was used both in the production of the MgO precursors or mixed oxides for the suspension and in the educt mixture for catalytic testing, was provided by the GENO-OSMO WK 1–50 reverse osmosis plant from Grünbeck (Hoechstaedt a. d. Donau, Germany). Non-denatured ethanol (purity: >99.5 vol%) from Berkel AHK (Ludwigshafen, Germany), was used for the catalytic tests.

3.2. Preparation of Binary MgO/SiO_2 Mixed Oxides from Commercially Available Precursors

Initially, binary mixtures of MgO and SiO_2 with various molar compositions were produced. The MgO precursor M1 was obtained by calcination for 4 h at 900 °C from $Mg(OH)_2$. Highly disperse silica (Wacker Silicones, HDK N20) was used as SiO_2 precursor.

A total mass of 10 g of the oxidic precursors was weighed into a 500 mL round flask and suspended with deionized water at 2.5 times the volume of the bulk volume of the solids. The suspension was homogenized at 70 °C and 800 mbar for 30 min in a rotary evaporator and then concentrated at 170 mbar. After drying overnight at 70 °C in the drying chamber, calcination was carried out at 500 °C for 6 h in an air stream (heating rate 1.2 K/min). The powder obtained was pressed into tablets under 15–20 bar, then mortarized and classified. For the catalytic tests, the particle fraction of 200 to 400 µm was used.

3.3. Preparation of Binary MgO/SiO_2 Mixed Oxides with Mesoporous MgO

The mesoporous MgO precursors M2 and M3 were produced according to the method presented by Cui et al. [35]. First, 500 mL of a $Mg(NO_3)_2$ solution (0.624 mol/L) were placed in a 1 L round flask. Then, 250 mL of a carbonate solution (Na_2CO_3 or K_2CO_3, each 1.248 mol/L) were added via a dropping funnel at a rate of two drops per second using a magnetic stirrer. Precipitation and subsequent homogenization for 30 min took place at room temperature. The precipitation suspension was then hydrothermally treated at 180 °C in an autoclave (2 L capacity). The duration of the autoclave treatment was varied (0 h, 5 h, 9 h, 12 h, 24 h, and 48 h) and is indicated in brackets behind the precursor name in Section 2.2. The aged precipitated suspension was filtered, washed with deionized water, and dried overnight at 70 °C. The precipitated $MgCO_3$ was converted to MgO by calcination at 600 °C for 2 h (heating rate 5 K/min). The MgO precursor M2 was prepared with Na_2CO_3, the precursor M3 with K_2CO_3.

To produce the mixed oxide, the respective mesoporous MgO precursor was mixed with SiO_2 using the mechanical stirrer FL-300 MS (FLUID Misch- und Dispergiertechnik GmbH, Loerrach, Germany). For this purpose, 4.282 g M2 or M3 and 0.718 g SiO_2 (molar Mg/Si ratio of 90:10) were suspended with 200 mL deionized water. The aqueous suspension was homogenized at 400 rpm and 70 °C for 30 min. The temperature was then raised to 95 °C, the stirring speed was reduced to 300 rpm,

and the suspension was concentrated for about 30 min. The further preparation steps of drying, calcination, pressing, and classification were carried out in the same way as described in Section 3.2.

3.4. Characterization of MgO/SiO_2 Mixed Oxides and Precursors

The prepared mixed oxides and the respective precursors were characterized texturally by the specific BET surface areas S_{BET} and pore volumes V_p calculated from nitrogen physisorption at 77 K (Sorptomatik 1990, Carlo Erba Instruments, Egelsbach, Germany). Prior to the adsorption experiment, the solid samples were treated under standard conditions by heating to 250 °C under high vacuum with a heating rate of 1 K/min and maintaining at this temperature for 8 h.

The surface acidity of the mixed oxides and the corresponding precursors was determined using temperature-programmed ammonia desorption (NH_3-TPD) (TPDRO 1100, Thermo Scientific, Milan, Italy). During the analysis, the samples were heated to 450 °C at 10 K/min in a helium stream. The desorbed ammonia was detected with a thermal conductivity detector. Assuming that the ammonia load N_{NH_3} corresponds to the number of acid sites on the solid surface, the acid-site density ρ_{as} follows from the quotient of the specific ammonia load N_{NH_3} and the specific surface area S_{BET}.

The morphology of the solid samples was examined by scanning electron microscopy (DSM 982 GEMINI, Carl Zeiss, Jena, Germany).

3.5. Catalytic Testing

The activity and selectivity during the conversion of ethanol were determined for the prepared MgO/SiO_2 mixed oxides. A multiple reactor plant consisting of six identically constructed reactor lines was used [36]. The sample was taken from one of the six product streams via a multi-position valve and then automatically injected into the gas chromatograph. The flow diagram of one of the six reactor lines is shown in Figure A4.

The liquid educt mixture of 94 wt% ethanol and 6 wt% deionized water was placed in a reservoir. The volume flows of the liquid educt mixture and the carrier gas were controlled by two mass flow controllers and fed through a flow tube reactor (Bergmann RST, Dresden, Germany, stainless steel, 14 mm inner diameter) filled with 500 mg of the mixed oxide catalyst (particle size 200–400 µm) between two layers of quartz glass wool. The catalyst load (weight hourly space velocity (WHSV)) during the test results from the ratio of the educt mass flow to the catalyst mass.

An electric heating element was used to heat the reactor, whereby the temperature was measured directly above the catalyst sample. Temperature programs of different durations were used for catalytic testing. After 8.75 h at 400 °C, the reactor was heated up to 450 °C within 15 min and then maintained at this temperature for 8 to 17 h. Finally, a temperature of 400 °C was set again for 7 h (see Figure A5). Each catalyst was only tested once. All lines upstream of the reactor were heated to 120 °C, and those between the reactor outlet and the gas chromatograph to 200 °C.

The qualitative and quantitative analysis of the reaction products was performed by means of a 7820A gas chromatograph (Agilent, Santa Clara, CA, USA) with a flame ionization detector and a non-polar J&W HP-1 19091Z-530 separation column (Agilent, Santa Clara, CA, USA). The gas chromatographic analyses of the product flow at 450 °C reactor temperature were carried out between 1 and 17 h after reaching 450 °C. The obtained conversions and selectivities represent average values from several gas chromatographic measurements.

4. Conclusions

In the present work, binary MgO/SiO_2 mixed oxides were prepared in different ways and characterized by means of N_2-adsorption, SEM, and NH_3-TPD. Their catalytic activity during the conversion of ethanol to 1,3-butadiene was evaluated. The molar composition and the carbonate source as well as the duration of the hydrothermal treatment during the preparation of the MgO precursors for the synthesis of the mixed oxides were varied.

It was shown that binary MgO/SiO_2 mixed oxides from commercially available precursors exhibit an optimum yield of 1,3-butadiene at a MgO content of 85–95 mol%. This confirms qualitatively the necessary excess of the basic component in the mixture described in the literature.

The pure oxides MgO and SiO_2 showed only a very small number of active acid sites and thus only a low catalytic activity. The number of active sites increased only when both components were mixed in aqueous suspension, while at the same time the surface texture was changed. More acid sites were formed as the specific surface area of the structure-determining magnesium oxide increased. A maximum value of the acid-site density was obtained with equimolar to magnesium-rich MgO/SiO_2 mixed oxides.

The precipitation of $MgCO_3$ and subsequent hydrothermal treatment of the precipitated suspension successfully produced mesoporous magnesium oxide with comparatively large specific BET surface areas. The $MgCO_3$ platelets grew with increasing treatment time in the autoclave and formed a secondary pore system, as confirmed by SEM images. Different carbonate sources influenced the textural and surface chemical properties of the MgO precursor and the resulting mixed oxide.

The temperature influence of the hydrothermal treatment on the $MgCO_3$ structure and thus the catalytic activity of the resulting mixed oxide during the conversion of ethanol to 1,3-butadiene is the subject of later investigations.

Author Contributions: Conceptualization, W.R.; methodology, W.R.; investigation, M.H. and F.A.; data curation, M.H. and F.A.; formal analysis, M.K.; writing—original draft, M.H.; writing—review and editing, all authors; supervision, W.R. and G.K.; funding acquisition, G.K. and W.R. All authors have read and agreed to the published version of the manuscript.

Funding: This research was funded by Lanxess AG and SMWK (MatEnUm1-TP 4). Open Access Funding was provided by the Publication Fund of the TU Dresden.

Acknowledgments: The authors wish to thank Maik Bernhard and Axel Thomas for the design of the multiple reactor plant for catalytic testing, which was used to generate the catalytic results shown in this paper.

Conflicts of Interest: The authors declare no conflict of interest. The funders had no role in the writing of the manuscript or in the decision to publish the results.

Appendix A

Table A1. Processing of 1,3-butadiene, its end products, and their use [4].

Processing	End Product	Use
Polymerization	Polybutadiene (PBR)	Tires
Copolymerization with styrene	Styrene-butadiene rubber (SBR)	Tires
	Styrene-butadiene latex (SBL)	Paper coating
Copolymerization with acrylonitrile	Nitrile-butadiene rubber (NBR)	Seals, gloves
Copolymerization with acrylonitrile and styrene	Acrylonitrile butadiene styrene plastics (ABS)	Components in the electronics and automotive industries
Conversion with prussic acid to adiponitrile and subsequent hydrogenation	Hexamethylene diamine	Nylon-6,6
Conversion with chlorine to chloroprene and subsequent polymerization	Polychloroprene (neoprene)	Clothes

Table A2. Characterization results of the textural and surface acid investigations on the binary $M1/SiO_2$ mixed oxides and the precursors M1 and SiO_2, shown in Figure 5.

MgO Content (mol%)	0	25	50	75	85	90	100
S_{BET} (m^2/g)	185	432	391	90	143	98	174
N_{NH_3} (µmol/g)	39	739	843	196	225	153	7
ρ_{as} (nmol/m^2)	211	1711	2156	2178	1573	1561	40

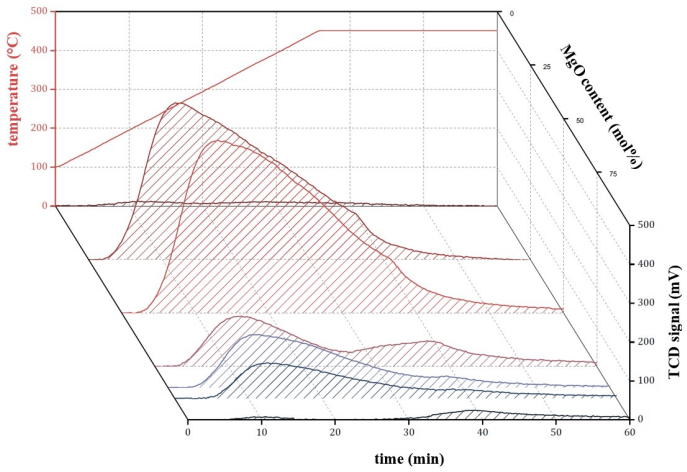

Figure A1. Temperature-programmed ammonia desorption (NH_3-TPD) profiles of M1 (pure), SiO_2 (pure), and binary M1/SiO_2 catalyst samples with various compositions.

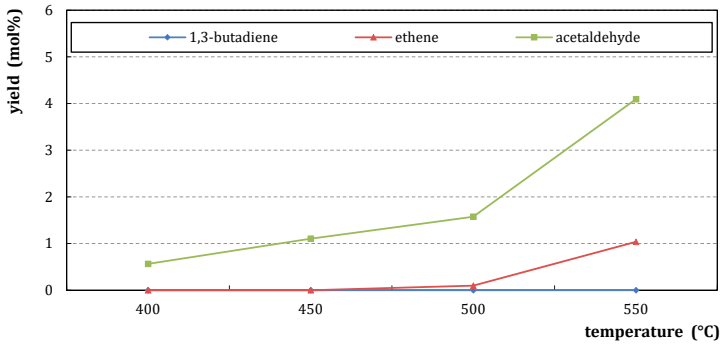

Figure A2. Results of the blank tests at different temperatures without catalyst sample in the reactor ($\dot{m}_{EtOH}$ = 2.8 g/h; p = 5.5 bar(a); $\dot{V}_{N_2}$ = 5 L/h).

The yield Y of product i is calculated as follows:

$$Y_i = \frac{X \cdot S_i}{100\%}. \quad \text{(A1)}$$

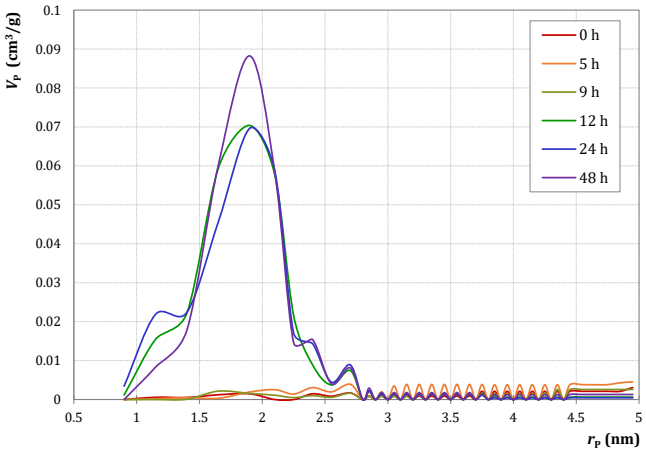

Figure A3. BJH pore radius distribution of M3/SiO_2 90:10 mixed oxide samples with different autoclave treatment durations.

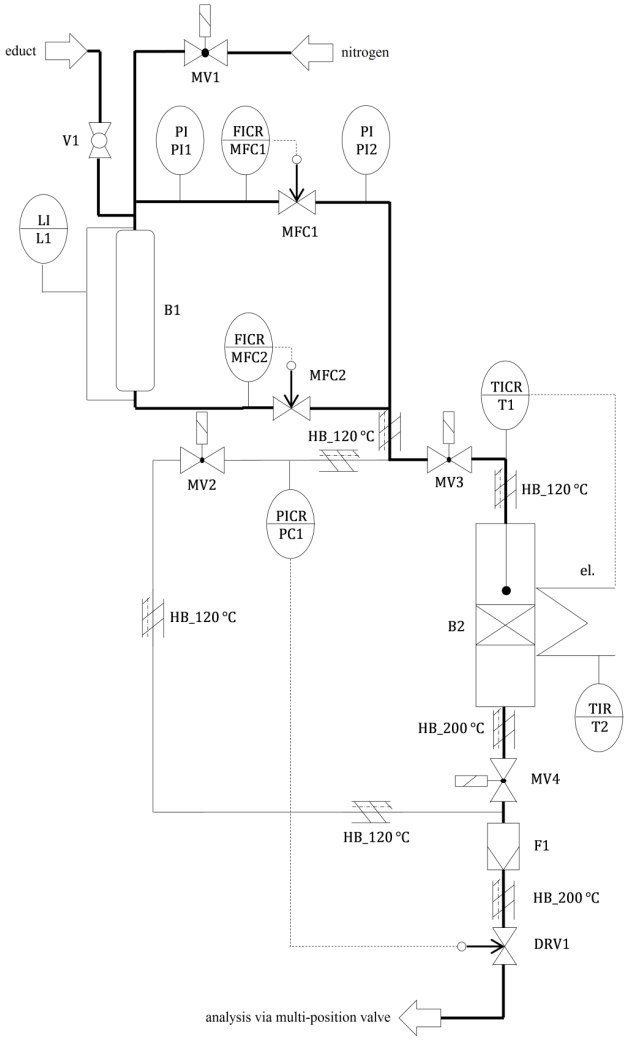

Figure A4. Flow diagram of a reactor line of the multiple reactor plant used.

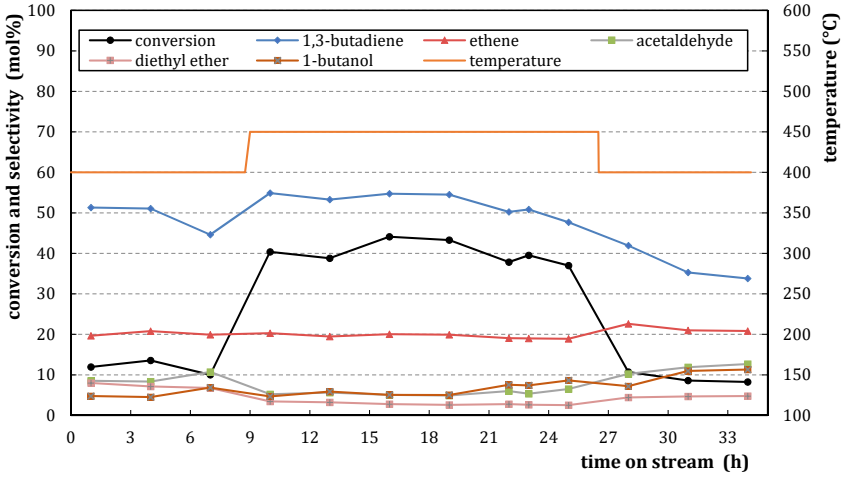

Figure A5. Results of catalytic testing of M3(24)/SiO_2 90:10; produced according to Section 3.3. with 24 h autoclave treatment duration (m_{cat} = 500 mg; WHSV = 4.7 h^{-1}; T = 450 °C; p = 5.5 bar(a); $\dot{V}_{N_2}$ = 5 L/h). The catalyst showed only very little deactivation.

References

1. Organization of the Petroleum Exporting Countries OPEC, World Oil Outlook 2014. Available online: https://www.opec.org/opec_web/en/publications/3049.htm (accessed on 7 June 2020).
2. Reschetilowski, W.; Schmidt, M. Bioethanol im Fokus der nachhaltigen Energie- und Chemiewirtschaft. *Wiss. Z. TU Dresd.* **2007**, *56*, 73–78.
3. Kalkman, J.; Pfeiffer, W.; Pereira, S. Are We Running out of Oil? Available online: https://www.rolandberger.com/fr/Publications/Are-we-running-out-of-oil.html (accessed on 7 June 2020).
4. White, W. Butadiene production process overview. *Chem. Biol. Interact.* **2007**, *166*, 10–14. [CrossRef] [PubMed]
5. Malaysian Rubber Board LGM, NR Statistics 2019. Available online: http://www.lgm.gov.my/general/General.aspx (accessed on 7 June 2020).
6. Weissermel, K.; Arpe, H.J. *Industrielle Organische Chemie*; Wiley-VCH: Weinheim, Germany, 1998.
7. Fedtke, M.; Pritzkow, W.; Zimmermann, G. *Technische Organische Chemie*; Deutscher Verlag für Grundstoffindustrie: Leipzig, Germany, 1992.
8. Bruijnincx, P.; Weckhuysen, B. Shale gas revolution: An opportunity for the production of biobased chemicals? *Angew. Chem. Int. Ed. Engl.* **2013**, *52*, 11980–11987. [CrossRef] [PubMed]
9. Angelici, C.; Weckhuysen, B.; Bruijnincx, P. Chemocatalytic conversion of ethanol into butadiene and other bulk chemicals. *ChemSusChem* **2013**, *6*, 1595–1614. [CrossRef]
10. Hirschberg, H. *Handbuch Verfahrenstechnik und Anlagenbau*; Springer: Berlin/Heidelberg, Germany, 1999.
11. Lebedew, S. Preparation of bivinyl directly from alcohol. *Zh. Obshch. Khim.* **1933**, *3*, 698–717.
12. Kvisle, S.; Aguero, A.; Sneeden, R. Transformation of ethanol into 1,3-butadiene over magnesium oxide/silica catalysts. *Appl. Catal.* **1988**, *43*, 117–131. [CrossRef]
13. León, M.; Diaz, E.; Ordóñez, S. Ethanol catalytic condensation over Mg-Al mixed oxides derived from hydrotalcites. *Catal. Today* **2011**, *164*, 436–442. [CrossRef]
14. Ezinkwo, G.; Tretjakov, V.; Aliyu, A.; Ilolov, A. Fundamental Issues of Catalytic Conversion of Bio-Ethanol into Butadiene. *ChemBioEng. Rev.* **2014**, *1*, 194–203. [CrossRef]
15. Jones, M. Catalytic transformation of ethanol into 1,3-butadiene. *Chem. Cent. J.* **2014**, *8*, 53. [CrossRef]
16. Makshina, E.; Dusselier, M.; Janssens, W.; Degrève, J.; Jacobs, P.; Sels, B. Review of old chemistry and new catalytic advances in the on-purpose synthesis of butadiene. *Chem. Soc. Rev.* **2014**, *43*, 7917–7953. [CrossRef]
17. Brückner, R. *Reaktionsmechanismen*; Springer: Berlin/Heidelberg, Germany, 2004.
18. Makshina, E.; Janssens, W.; Sels, B.; Jacobs, B. Catalytic study of the conversion of ethanol into 1,3-butadiene. *Catal. Today* **2012**, *198*, 338–344. [CrossRef]
19. Bhattacharyya, S.; Sanyal, S. Kinetic study on the mechanism of the catalytic conversion of ethanol to butadiene. *J. Catal.* **1967**, *7*, 152–158. [CrossRef]
20. Di Cosimo, J.; Acosta, A.; Apesteguía, C. Gas-phase hydrogen transfer reduction of α,β-unsaturated ketones on Mg-based catalysts. *J. Mol. Catal. A Chem.* **2004**, *222*, 87–96. [CrossRef]
21. Niiyama, H.; Morii, S.; Echigoya, E. Butadiene formation from ethanol over silica-magnesia catalysts. *Bull. Chem. Soc. Jpn.* **1972**, *45*, 655–659. [CrossRef]
22. Lebedev, S. Improvements in or Relating to the Preparation of Diolefines Directly from Alcohols. Patent GB 331482A, 30 June 1931.
23. Szukiewicz, W. Method for Producing Butadiene. Patent US 2357855A, 12 September 1944.
24. Corson, B.; Jones, H.; Welling, C.; Hinckley, J.; Stahly, E. Butadiene from Ethyl Alcohol. Catalysis in the One- and Two-Stop Processes. *Ind. Eng. Chem.* **1950**, *42*, 359–373. [CrossRef]
25. Ohnishi, R.; Akimoto, T.; Tanabe, K. Pronounced catalytic activity and selectivity of MgO-SiO_2-Na_2O for synthesis of buta-1,3-diene from ethanol. *J. Chem. Soc. Chem. Commun.* **1985**, *70*, 1613–1614. [CrossRef]
26. Suzuki, E.; Idemura, S.; Ono, Y. Catalytic conversion of 2-propanol and ethanol over synthetic hectorite and its analogues. *Appl. Clay Sci.* **1988**, *3*, 123–134. [CrossRef]
27. Lewandowski, M.; Babu, G.; Vezzoli, M.; Jones, M.; Owen, R.; Mattia, D.; Plucinski, P.; Mikolajska, E.; Ochenduszko, A.; Apperley, D. Investigations into the conversion of ethanol to 1,3-butadiene using MgO:SiO_2 supported catalysts. *Catal. Commun.* **2014**, *49*, 25–28. [CrossRef]
28. Haufe, R.; Reschetilowski, W.; Thomas, A.; Hauser, M. Process for the Production of 1,3-butadiene. Patent EP 2 918 338 A1, 16 September 2015.

29. Kovařík, B. Einfluss der Magnesiumsilikate auf die Aktivität des Lebedew-Katalysators. *Collect. Czech. Chem. Commun.* **1961**, *26*, 1918–1924. [CrossRef]
30. Huang, X.; Men, Y.; Wang, J.; An, W.; Wang, Y. Highly active and selective binary MgO-SiO_2 catalysts for the production of 1,3-butadiene from ethanol. *Catal. Sci. Technol.* **2017**, *7*, 168–180. [CrossRef]
31. Taifan, W.; Baltrusaitis, J. In Situ Spectroscopic Insights on the Molecular Structure of the MgO/SiO_2 Catalytic Active Sites during Ethanol Conversion to 1,3-Butadiene. *J. Phys. Chem. C* **2018**, *122*, 20894–20906. [CrossRef]
32. Li, S.; Men, Y.; Wang, J.; Liu, S.; Wang, X.; Ji, F.; Chai, S.; Song, Q. Morphological control of inverted MgO-SiO_2 composite catalysts for efficient conversion of ethanol to 1,3-butadiene. *Appl. Catal. A Gen.* **2019**, *577*, 1–9. [CrossRef]
33. Abdulrazzaq, H.; Chokanlu, A.; Frederick, B.; Schwartz, T. Reaction Kinetics Analysis of Ethanol Dehydrogenation Catalyzed by MgO-SiO_2. *ACS Catal.* **2020**, *10*, 6318–6331. [CrossRef]
34. Thommes, M.; Kaneko, K.; Neimark, A.; Olivier, J.; Rodriguez-Reinoso, F.; Rouquerol, J.; Sing, K. Physisorption of gases, with special reference to the evaluation of surface area and pore size distribution (IUPAC Technical Report). *Pure Appl. Chem.* **2015**, *87*, 1051–1069. [CrossRef]
35. Cui, H.; Wu, X.; Chen, Y.; Boughton, R. Synthesis and characterization of mesoporous MgO by template-free hydrothermal method. *Mater. Res. Bull.* **2014**, *50*, 307–311. [CrossRef]
36. Thomas, A. Reaktionstechnische und Mechanistische Untersuchungen der Umsetzung von Ethanol zu 1,3-Butadien an Mischoxidkatalysatoren. Ph.D. Thesis, Dresden University of Technology, Dresden, Germany, 21 November 2015.